An Air–Sea Coupled Skeleton Model for the Madden–Julian Oscillation*

FEI LIU AND BIN WANG

International Pacific Research Center, and Department of Meteorology, University of Hawai'i at Mānoa, Honolulu, Hawaii

(Manuscript received 18 December 2012, in final form 20 May 2013)

ABSTRACT

This work is an extension and improvement of the minimal Madden–Julian oscillation (MJO) ''skeleton'' model developed by Majda and Stechmann, which can capture some important features of the MJO—slow eastward propagation, quadrupole-vortex structure, and independence of frequency on wavelength—but is unable to produce unstable growth and selection of eastward-propagating planetary waves. With the addition of planetary boundary layer frictional moisture convergence, these deficiencies can be remedied. The frictional boundary layer ''selects'' the planetary-scale eastward propagation as the most unstable mode, but the dynamics remains confined to atmospheric processes only. Here the authors study the role of air–sea interaction by implementing an oceanic mixed-layer (ML) model of Wang and Xie into the MJO skeleton model. In this new air–sea coupled skeleton model, the features of the original skeleton model remain; additionally, the air–sea interaction under mean westerly winds is shown to produce a strong instability that selectively destabilizes the eastward-propagating planetary-scale waves. Although the cloud–shortwave radiation–sea surface temperature (CRS) feedback destabilizes both eastward and westward modes, the air–sea feedback associated with the evaporation and oceanic entrainment favors planetary-scale eastward modes. Over the Western Hemisphere where easterly background winds prevail, the evaporation and entrainment feedbacks yield damped modes, indicating that longitudinal variation of the mean surface winds plays an important role in regulation of the MJO intensity in addition to the longitudinal variation of the mean sea surface temperature or mean moist static stability. This theoretical analysis suggests that accurate simulation of the climatological mean state is critical for capturing the realistic air–sea interaction and thus the MJO.

1. Introduction

The Madden–Julian oscillation (MJO), named after its discoverers (Madden and Julian 1971), features an equatorially trapped, slowly eastward-propagating (about 5 m s^{-1}), planetary-scale baroclinic circulation cell in the Eastern Hemisphere (Knutson and Weickmann 1987; Wang and Rui 1990a; Hendon and Salby 1994; Maloney and Hartmann 1998; Kiladis et al. 2005; Zhang 2005). The MJO circulation comprises equatorial Kelvin waves and Rossby waves and exhibits a quadrupole-vortex-like horizontal structure when the MJO convection is located over the equatorial Indian Ocean and the western Pacific (Rui and Wang 1990; Hendon and Salby 1994). In addition, strong development of MJO convective anomalies has been found in the equatorial Indian Ocean and western Pacific while decaying over the eastern Pacific and the Maritime Continent (Wang and Rui 1990a). In the phase space, the MJO frequency does not depend on wavenumber (Salby and Hendon 1994; Wheeler and Kiladis 1999; Roundy and Frank 2004).

Based on the multiscale structure of MJO (Nakazawa 1988; Houze et al. 2000; Slingo et al. 2003; Moncrieff 2004; Kikuchi and Wang 2010), in which the primary instabilities and damping are assumed to occur on synoptic scales (Khouider and Majda 2006, 2008), Majda and Stechmann (2009, hereafter MS09) built a minimal dynamical model for the MJO, called the MJO ''skeleton'' model, which captures three important features of the MJO—slow eastward propagation at a speed of roughly 5 m s^{-1} (Fig. 1b); a peculiar dispersion relation of $d\sigma/dk \approx 0$ (Fig. 1a), where σ and k are the frequency and wavenumber, respectively; and a quadrupole-vortex

* School of Ocean and Earth Science and Technology Contribution Number 8946 and International Pacific Research Center Publication Number 986.

Corresponding author address: Dr. Bin Wang, IPRC and Department of Meteorology, University of Hawai'i at Mānoa, 401 POST Bldg, 1680 East-West Road, Honolulu, HI 96822.
E-mail: wangbin@hawaii.edu

DOI: 10.1175/JAS-D-12-0348.1

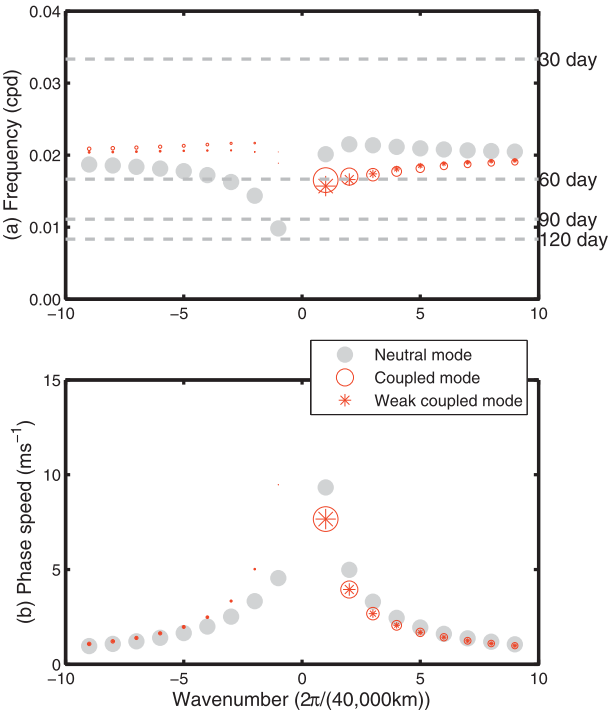

FIG. 1. Growth rate and speed of the coupled skeleton mode. (a) Frequency and (b) phase speed as functions of wavenumber for the low-frequency skeleton model without the frictional boundary layer. Gray dots denote results of MS09, which have no air–sea coupling and show only neutral modes (zero growth rates). Circles denote results derived from the coupled ocean-skeleton model, which shows unstable modes; the stars are the same as circles, except for a weaker coupling coefficient ($\eta_T = 6\,\mathrm{kg\,s^{-3}\,K^{-3}}$). The growth rates are proportional to the diameters, with respect to the maximum and minimum growth rates of 0.08 and 0.01 day^{-1}, respectively.

horizontal structure (see Fig. 2a). Observations show that the MJO convective activity and associated mesosynoptic waves develop over the equatorial Indian Ocean and western Pacific, indicating that MJO is possibly an unstable mode. The strength of MJO can be measured by the outgoing longwave radiation (OLR) anomalies at the MJO convective envelope. Amplification of MJO convection may imply a growth of MJO available potential energy or instability. It is interesting to explain why the MJO can grow or be maintained against atmospheric thermal and momentum damping and why the MJO prefers the planetary scale and eastward propagation.

The inclusion of a frictional planetary boundary layer can remedy these deficiencies (Liu and Wang 2012a, hereafter LW12). They show that the boundary layer frictional convergence provides a strong instability source for the long eastward-propagating modes, although it also destabilizes very short westward modes. The Ekman pumping moistens the low troposphere to the east of the MJO convective envelope and sets up favorable moist conditions to destabilize the MJO and favor only eastward modes. The sea surface temperature (SST) with a maximum at the equator also prefers the long eastward modes.

The MJO is not a phenomenon of the atmosphere alone; it also perturbs the upper ocean (e.g., Krishnamurti et al. 1988; Zhang 1996; Hendon and Glick 1997; Lau and Sui 1997; Jones et al. 1998), and the air–sea coupling may be an important part of the MJO dynamics (Flatau et al. 1997; Waliser et al. 1999; Inness et al. 2003). Wang and Xie (1998) advanced a theoretical model to demonstrate that the air–sea interaction can destabilize the moist Kelvin waves and Rossby waves associated with the MJO. Hence, besides the destabilization of the frictional boundary layer, it would be interesting to find out the role of the air–sea interaction in the MJO skeleton dynamics. The present study aims to elaborate the importance of the atmosphere–ocean interaction in MJO dynamics.

2. Air–sea coupled model

a. *Frictional atmospheric model*

The atmospheric model for planetary-scale motion was based on the frictional skeleton model developed by LW12, which was originally built by MS09, in which the effect of synoptic wave activity (and upscale eddy moisture and heat transfer) was crucially parameterized in the temperature and moisture equations. These parameterized eddy transport effects provide an oscillation mechanism in the MJO skeleton model (Liu and Wang 2012b, 2012c). The model is formulated in terms of anomalies from a uniform basic state of radiative–convective equilibrium. The interaction between the planetary-scale moisture and synoptic wave activity was parameterized by assuming that positive lower-tropospheric moisture anomaly favors the growth of synoptic-scale wave activity (Majda and Stechmann 2011). The frictional boundary layer will pump additional moisture to the free troposphere (LW12). Meanwhile, the SST will also affect the atmosphere (Wang and Li 1993; Liu and Wang 2012d), in which parameterized are various processes by which SST affects the atmosphere, including through its impact on convective heating (Philander et al. 1984; Hirst 1986), heating associated with evaporation (Zebiak 1986), longwave Newtonian relaxation (Davey and Gill 1987), and the equivalent SST gradient effect (Lindzen and Nigam 1987; Neelin 1989). The linear equations for the first baroclinic mode can be written as

$$
\begin{aligned}
U_t - \beta y V + \phi_x &= 0,\\
\beta y U + \phi_y &= 0,\\
\phi_t + C_0^2(U_x + V_y) &= -\frac{R\Delta p}{C_p p_2} a - \frac{Rg}{2C_p p_2}\eta_T T,\\
q_t + p_2\tilde{Q}(U_x + V_y) &= -\frac{1}{L_C} a + \frac{g}{\Delta p L_C}\eta_E T\\
&\quad + r_b(\overline{T} - 9.18)w_b, \quad \text{and}\\
a_t &= \Gamma\overline{a} q, \qquad (1)
\end{aligned}
$$

where U and V are the anomalous zonal (x) and meridional (y) velocities, T is the SST, ϕ is the geopotential, $\overline{T}$ is the mean SST, C_0 is the gravest gravity wave speed, β is the leading-order curvature effect of Earth at the equator, R is the specific gas constant, C_p is the specific heat at constant pressure, L_C is the latent heat of condensation, g is the gravity acceleration, Δp and p_2 are the tropospheric depth and midtropospheric height, respectively, η_T is the SST forcing parameter, η_E is the latent heating coefficient, $\tilde{Q}$ is the vertical gradient of the background moisture, $\overline{a}$ is the mean wave activity, and Γ is the constant of proportionality.

The additional moisture source pumped by the frictional boundary layer is represented by the last term of the moisture equation. The boundary transfer parameter is r_b, which is set to zero when neglecting the role of frictional boundary layer. The Ekman pumping can be calculated from the steady boundary layer model (LW12):

$$w_b = r_d(d_1\nabla^2\phi + d_2\phi_x + d_3\phi_y), \qquad (2)$$

where r_d is the depth ratio of boundary layer to troposphere, and the same value as in LW12 has been used. The Ekman coefficients are $d_1 = E/(E^2 + \beta^2 y^2)$, $d_2 = -(\beta E^2 - \beta^3 y^2)/(E^2 + \beta^2 y^2)^2$, and $d_3 = -2\beta E y/(E^2 + \beta^2 y^2)^2$.

b. Mixed-layer (ML) model

In the warm-pool region where the MJO prevails, the thermocline is deep and horizontal SST gradients are small, and the ocean wave dynamics are not critical to SST changes (Wang and Xie 1998), thus we use a simple ML model developed by Wang and Xie (1998). This model was distilled from the 2.5-layer ocean model of Wang et al. (1995) and include three processes that affect the SST over the warm-pool region: 1) the cloud–shortwave radiation–SST (CRS) feedback associated with the wave activity, 2) the entrainment feedback through turbulence mixing in the bottom of the ML, and 3) the evaporation feedback through changing the sea surface latent heat flux. The linearized ML model can be written as [Eq. (3.1) of Wang and Xie (1998)]

$$
\begin{aligned}
h_{1t} &= E_M\overline{U}U + \overline{w}_e\left(\frac{3U}{\overline{U}} - \frac{H}{H_2}\frac{h_1}{H_1}\right),\\
T_t &= -D_{\text{rad}}a - D_{\text{ent}}\left(\frac{3U}{\overline{U}} - \frac{h_1}{H_1}\right)\\
&\quad - D_{\text{eva}}\left(\frac{U}{\overline{U}} + \frac{T}{\overline{T} - 293}\right), \qquad (3)
\end{aligned}
$$

where h_1 is the anomalous ML depth, H_1 is the mean ML depth, $\overline{U}$ is the mean surface wind, $\overline{w}_e$ is the mean entrainment rate, H is the mean thermocline depth, $H_2 = H - H_1$, and E_M is the ML Ekman-pumping coefficient. The terms D_{rad}, D_{ent}, and D_{eva} are feedback coefficients associated with the CRS, entrainment and evaporation, respectively.

c. Model parameters

The atmospheric parameters are listed in Table 1. The latent heating coefficient can be written as $\eta_E = \rho_a C_E L_C K_q|\overline{U}|$, where $\rho_a = 1.2\,\text{kg m}^{-3}$ is the

TABLE 1. Parameter values used in the atmospheric model.

Name and value	Physical quantity
$C_0 = 50\,\text{m s}^{-1}$	Gravest gravity wave speed
$\Delta p = 400\,\text{hPa}$	Pressure depth of lower troposphere
$p_2 = 500\,\text{hPa}$	Middle-tropospheric pressure
$\tilde{Q} = 1.5\times10^{-4}\,\text{g kg}^{-1}\,\text{Pa}^{-1}$	Vertical gradient of the background moisture
$E = 3.9\times10^{-5}\,\text{s}^{-1}$	Boundary frictional coefficient
$r_d = 0.2$	Depth ratio of boundary to troposphere
$r_b = 5.2\times10^{-4}$	Boundary transfer parameter
$\Gamma\,\overline{a} = 5.1\times10^{-5}\,\text{m}^2\,\text{s}^{-3}$	Constant of proportionality
$\eta_T = 12\,\text{kg s}^{-3}\,\text{K}^{-3}$	SST forcing coefficient
$\eta_E = 12\,\text{kg s}^{-3}\,\text{K}^{-3}$	Latent heating coefficient

TABLE 2. Parameter values used in the ML model.

Name and value	Physical quantity
$A = 0.06$	Sea surface albedo
$S_0 = 320\,\text{W m}^{-2}$	Sea surface downward solar radiation flux under clear sky
$\gamma = 22.5\,\text{kg s J}^{-1}$	Cloud cover coefficient
$H_1 = 40\,\text{m}$	Mean ML depth
$H = 150\,\text{m}$	Mean thermocline depth
$E_M = 3.0\times10^{-7}\,\text{s}^{-1}$	ML Ekman pumping coefficient
$\overline{w}_e = 2\times10^{-6}$	Mean entrainment rate
$\overline{T} = 303\,\text{K}$	Mean SST
$\overline{T}_e = 301.2\,\text{K}$	Mean entrained water temperature
$D_{\text{rad0}} = 2.5\times10^{-5}\,\text{K s}^2\,\text{m}^{-2}$	ML CRS coefficient
$D_{\text{ent0}} = 0.9\times10^{-7}\,\text{K s}^{-1}$	ML entrainment coefficient
$D_{\text{eva0}} = 0.72\times10^{-7}\,\text{K s}^{-1}$	ML evaporation coefficient

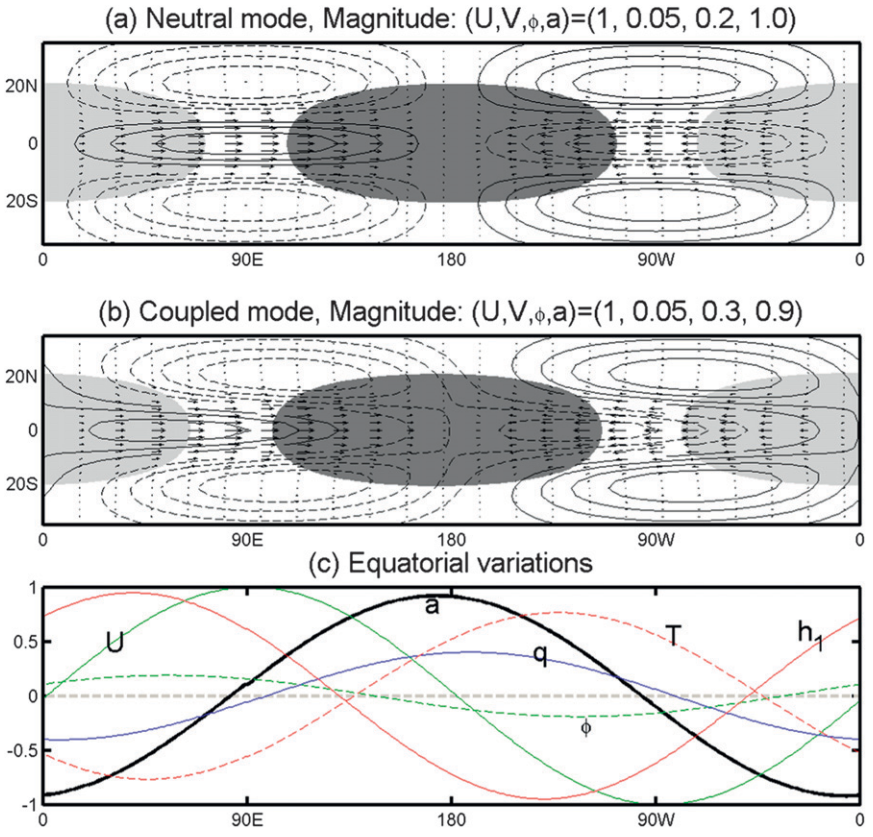

FIG. 2. Structure of the coupled skeleton mode. Velocity vectors, wave activity (shading), with lower-tropospheric geopotential (contours) of the (a) neutral mode of MS09 and (b) coupled mode in this study are plotted for eastward wavenumber 1. Positive (negative) contours are solid (dashed), and positive (negative) values are shaded dark (gray). Contour interval is one-fourth of the magnitude, and zero contours are not drawn. Only wave activity above one-third of the magnitude is shaded. (c) Equatorial zonal variations of wave activity (a), zonal wind (U), geopotential (ϕ), moisture (q), ML depth (h_1), and SST (T) for eastward wavenumber 1 of the coupled mode. The dimensional scales of these variations are 2.0 K day^{-1}, 6.25 m s^{-1}, 312 m^2 s^{-2}, 1.0 g kg^{-1}, 12.5 m, and 0.6 K, respectively.

surface air density, $C_E = 1.5 \times 10^{-3}$ is the moisture transfer coefficient, and $K_q = 8.9 \times 10^{-4}$ K^{-1}. For simplicity, the mean surface wind of $|\overline{U}| = 3$ m s^{-1} has been used for calculating the evaporation over the warm pool (Wang and Xie 1998), thus $\eta_E = 12$ kg s^{-3} K^{-3}. In this simple model we assume that the SST forcing has the same strength as the SST-induced evaporation, that is, $\eta_T = \eta_E$.

The ML $D_{\rm rad} = 0.622(1 - A)S_0\gamma/(\rho_0 C_w H_1)$ (Wang and Xie 1998), where A is the surface albedo, S_0 is the sea surface solar radiation flux under clear sky, ρ_0 is the water density, and C_W is the water heat capacity. The shortwave radiation is assumed to be proportional to the wave activity with a coefficient γ. The typical value $\gamma = 22.5$ kg s J^{-1} means that an anomalous precipitation of 1 mm day^{-1} may result in an increase in total cloudiness by one-tenth. The strong intraseasonal precipitation anomaly has an amplitude of about 10 mm day^{-1} (Wang et al. 2005). Assuming that a clear (cloudy) sky is associated with the dry (wet) phase of the MJO, a 10% increase of anomalous cloud cover corresponding to a 1 mm day^{-1} precipitation anomaly is reasonable for modeling MJO variability.

Also, $D_{\rm ent} = \overline{w}_e(\overline{T} - \overline{T}_e)/H_1$, where $\overline{T}_e$ is the mean entrained-water temperature, and $D_{\rm eva} = \eta_E(\overline{T} - 293)/\rho_0 C_w H_1$. Other ML parameters are listed in Table 2. Unless otherwise mentioned, $D_{\rm rad}$, $D_{\rm ent}$, and $D_{\rm eva}$ use the standard strength given in Table 2.

The constants include $R = 287$ J kg^{-1} K^{-1}, $C_p = 1004$ J kg^{-1} K^{-1}, $C_w = 4186$ J kg^{-1} K^{-1}, $\rho_0 = 1 \times 10^3$ kg m^{-3}, $L_C = 2.5 \times 10^6$ J kg^{-1}, the gravity acceleration $g = 9.8$ m s^{-2}, and the meridional Coriolis parameter variation $\beta = 2.3 \times 10^{-11}$ m^{-1} s^{-1}.

To highlight the role of air–sea interaction, the role of the frictional boundary layer has been removed first, that

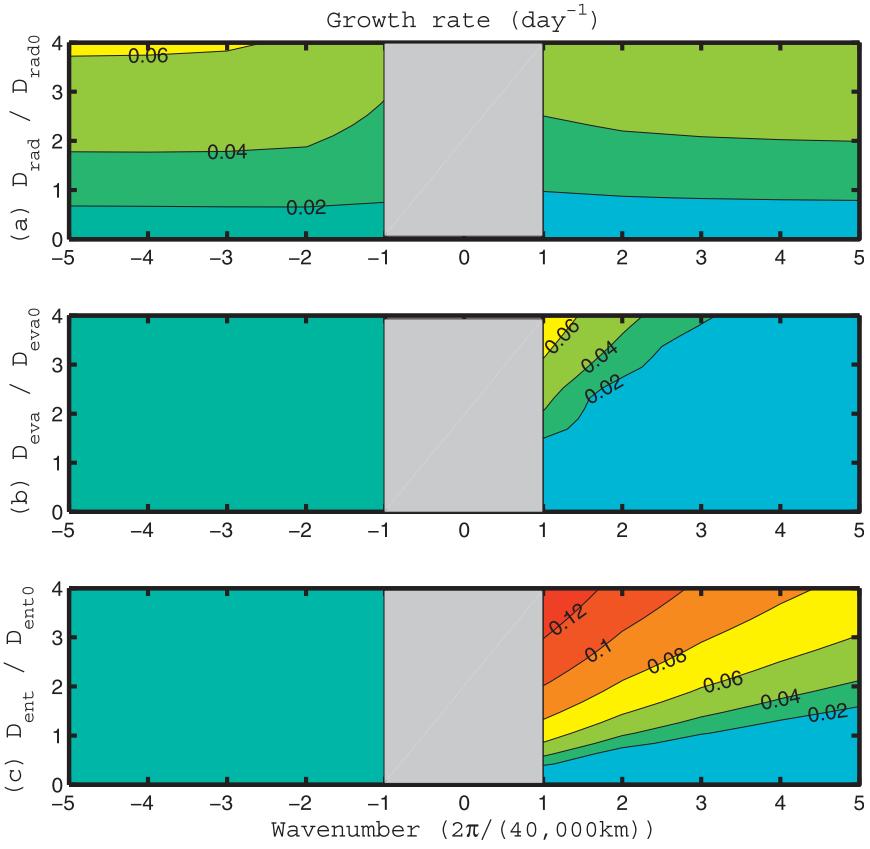

FIG. 3. Growth rate as functions of wavenumber and air–sea interaction strength associated with (a) the CRS feedback, (b) evaporation, and (c) entertainment for the coupled mode. In each experiment, the other two air–sea interaction processes are eliminated.

is, $r_b = 0$. (In Fig. 7 we include the frictional boundary layer by selecting non-zero r_b). The equatorially trapped SST has been used. The mean vertical moisture gradient and SST take the form of $\tilde{Q} = \tilde{Q}_0 \exp[-(y/y_L)^2]$ and $\overline{T} = \overline{T}_0 \exp[-(y/y_L)^2]$. The meridional damping scale is $y = 20°$, and the amplitudes are $\overline{T}_0 = 303\,\mathrm{K}$ and $\tilde{Q}_0 = 1.5 \times 10^{-4}\,\mathrm{g\,kg^{-1}\,Pa^{-1}}$.

d. Eigenvalue problem

Equations (1)–(3) form a linear air–sea coupled model, for which the eigenvalue problem can be readily solved. For the zonally propagating plane waves, we assume that they have the structure of $e^{i(kx-\sigma t)}$. The phase speed and growth rate are defined by $\mathrm{Re}(\sigma)/k$ and $\mathrm{Im}(\sigma)$, respectively.

When only the lowest N meridional modes of each variable are kept for the meridional expansion of parabolic cylinder functions, we project Eqs. (1)–(3) on the σ–k space and obtain a linear matrix of $(7N \times 7N)$ for the seven variables. Here, $N = 1$ represents the lowest equatorially trapped mode. The frequency and eigenvectors were calculated through matrix inversion for each wavenumber. Because of the longwave approximation in the free troposphere, only the Kelvin and Rossby waves are kept. Following the idea that the wave activity has only the lowest meridional truncation of parabolic cylinder functions (MS09), the Rossby and Kelvin waves, on their lowest meridional modes, can be studied by using $N = 3$, and sensitivity experiments show that a higher N does not affect the results.

3. Unstable coupled MJO skeleton

This air–sea coupled model still captures the skeleton of the MJO (Figs. 1 and 2b). Different from the neutral modes of MS09, the air–sea interaction provides an instability source for the coupled modes, which destabilizes both the westward and eastward modes. However, the air–sea interaction prefers providing the strongest instability source for the planetary-scale eastward-propagating modes, especially for the wavenumber-1 mode that has a strong growth rate of $0.08\,\mathrm{day^{-1}}$.

To sustain the growing modes, positive available potential energy should be generated, that is, positive

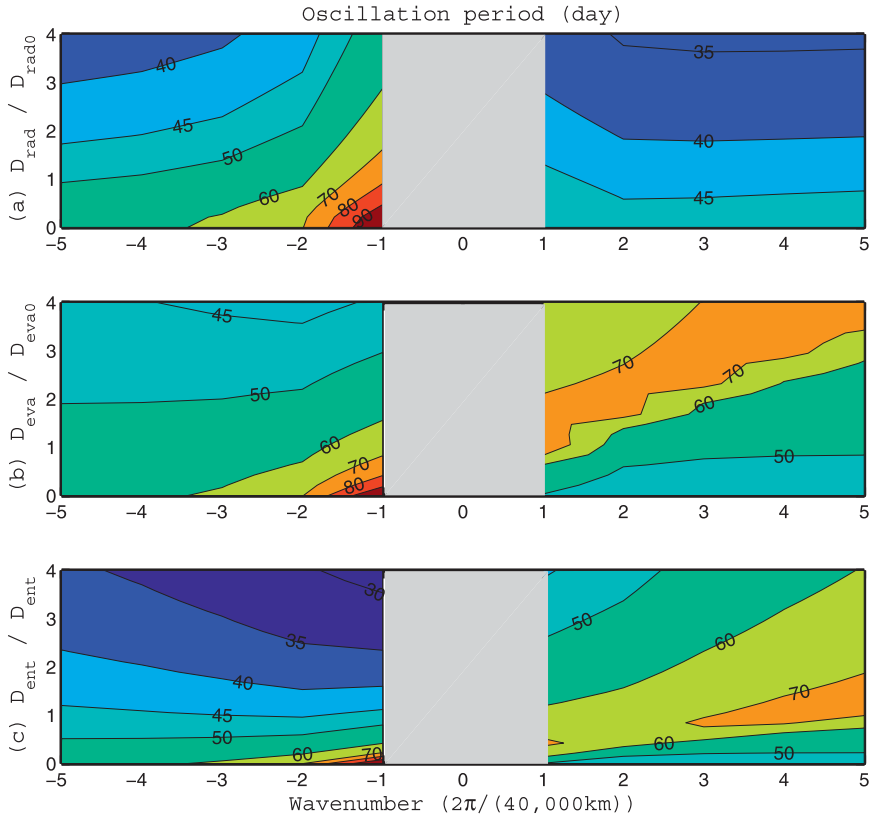

FIG. 4. As in Fig. 3, but for the oscillation period.

covariance between the perturbation temperature and wave activity is required (Wang and Rui 1990b). In the uncoupled model, only a symmetric quadrupole-vortex structure was produced (Fig. 2a), in which the temperature perturbations (out of phase with the geopotential anomaly) lead the wave activity by a phase of $\pi/2$, thus no available potential energy can be generated. In the coupled model, the air–sea interaction creates a zonal asymmetry, in which the positive temperature anomaly overlaps with positive wave activity field more than the negative temperature anomaly does (Fig. 2b), thus positive available potential energy is generated.

This positive covariance between the temperature and wave activity anomalies arises from the enhanced net heat flux release as a result of the positive SST in front of the MJO (Fig. 2c). First, the clear sky associated with the dry phase of MJO would enhance the short-wave radiation and warm the SST for the following wet phase of MJO. Second, the easterly wind anomaly to the east of the MJO center tends to reduce the mean evaporation and entrainment cooling against the mean westerly winds, which also produces a positive SST anomaly in front of the MJO. The total air–sea fluxes produce a positive SST anomaly that leads the MJO wave activity anomaly by a spatial phase of less than $\pi/4$, which is in good agreement with the observation (Kawamura 1988).

In the neutral mode of Majda and Stechmann (2009), the moisture anomaly leads the wave activity by 90°. While in the unstable coupled model, the air–sea interaction destroyed this asymmetry (Fig. 2b). From the moisture equation, the moisture tendency is affected by both the wave activity and wave convergence. The wave convergence is determined by the pressure anomaly and is not symmetric about the wave activity any more. Such an asymmetry will produce the moisture anomaly that just leads the wave activity by a phase less than 90°.

This simple model allows us to study the role of each of the three air–sea coupled processes. As shown in Fig. 3, the CRS feedback destabilizes both the eastward and westward modes, while the other two air–sea interactions associated with the evaporation and entrainment select the eastward wavenumber 1 as the most unstable mode. Wang and Xie (1998) also presented similar results for the moist Kelvin waves and Rossby waves associated with the MJO.

In the original skeleton model (Majda and Stechmann 2009), sensitivity experiments show that associated with

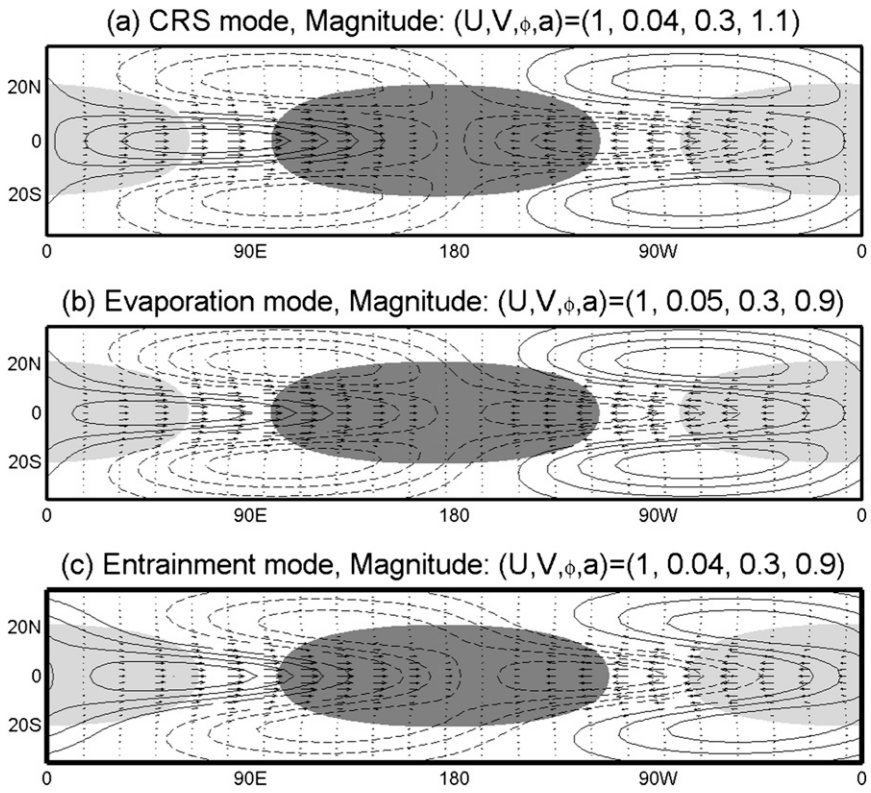

FIG. 5. Velocity vectors, wave activity (shading), with lower-tropospheric geopotential (contours) of the (a) strong CRS mode, $D_{rad}/D_{rad0} = 4$, (b) strong evaporation mode, $D_{eva}/D_{eva0} = 4$, and (c) strong entrainment mode, $D_{ent}/D_{ent0} = 4$; modes are plotted for eastward wavenumber 1. In each mode, the other two air–sea interactions are removed. Positive (negative) contours are solid (dashed), and positive (negative) values are shaded dark (gray). Contour interval is one-fourth of the magnitude, and zero contours are not drawn. Only wave activity above one-third of the magnitude is shaded.

the change in model parameters (i.e., background vertical moisture gradient $\bar{Q}$ and wave activity parameterization $\Gamma\overline{a}$), the change of wave amplitude is generally small, the quadrupole-vortex structure always exists, and the frequency remains to stay in the intraseasonal domain of 30–90 days, which means that the simulated MJO skeleton are robust over a wide range of atmospheric parameter values. With different air–sea interaction parameters (Fig. 3), the coupled model still maintains the MJO skeleton well. The model always simulates the low-frequency (30–90 days) oscillation (Fig. 4) and presents the pronounced quadrupole-vortex structure (Fig. 5). Furthermore, the increase of the SST forcing coefficient will enhance the model instability, but it does not change the frequency dramatically (Fig. 1a). These results show that the skeleton is still firm over a wide range of air–sea interaction, so it can hold the ''muscle'' of the MJO that will be attached to it in the future.

The MJO amplification appears to prefer lower-level and surface mean westerly winds in both numerical model simulations (Inness et al. 2003; Zhou et al. 2012) and observations (Wang and Rui 1990a; Zhang and Dong 2004). Our model also demonstrates the importance of the mean westerly winds in selecting the eastward planetary-scale mode. Under mean easterly winds, the air–sea interaction prefers westward-propagating modes in terms of instability (Fig. 6), which are attributable to the roles of evaporation and entrainment, because the westerly wind anomaly, located to the west of the wave activity center, would reduce the roles of evaporation and entrainment against the mean easterly winds and produce a positive SST anomaly to the west of the convection center, which prefers the westward unstable modes.

The unstable modes are attributable to two mechanisms: 1) the wind-induced surface heat exchange (WISHE) mechanism associated with entrainment and wind–evaporation feedbacks and 2) the atmosphere–ocean interaction associated with shortwave radiation feedback. Without the mean winds, the zonally symmetric wind-induced evaporation and entrainment feedbacks

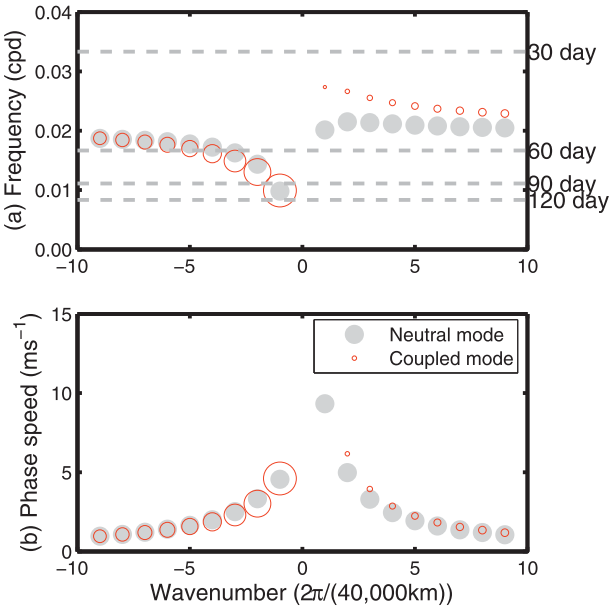

FIG. 6. As in Fig. 1, but for mean easterly winds of $\overline{U} = -3\,\mathrm{m\,s^{-1}}$. The maximum and minimum growth rates are 0.09 and 0.01 day^{-1}, respectively. The evaporation and entrainment feedbacks destabilize the westward propagation mode.

cannot produce unstable mode. However, the asymmetric CRS feedback can produce unstable modes because the clear sky associated with the dry phase always leaves a warm SST, which will destabilize the ensuing wet phase for both westward and eastward modes. These results mean that the mean-state winds will modulate the atmosphere–ocean interaction and affect growth rates.

Based on the above eigenvalue solutions, we conclude that the Eastern Hemispheric westerly winds present a favorable background state for the MJO, although the Eastern Hemispheric westerly winds only occur over a limited area of roughly one-third of the equatorial region. In observation, the MJO convective complex has a typical length scale of a few thousands kilometers, and the circulation has a planetary scale. The air–sea interaction matters mostly in the vicinity of convective complex. Strong development of MJO convective anomalies are found in the equatorial Indian Ocean and western Pacific where mean westerly winds prevail, whereas the MJO convective anomalies decay over the eastern Pacific where mean easterly winds prevail (Wang and Rui 1990a). If we consider the core portion of the MJO, then the length scale may marginally fit into the two mean wind regimes. The mismatch between convective complex and circulation is due to the effect of nonlinear (positive) heating. The nonlinear heating constrains the convective complex on a large scale but the fast dry Kelvin and Rossby waves propagate away from the convective complex and fill in the entire tropics, forming planetary-scale circulation anomalies (Wang and Li 1994). Here, we perform a linear analysis, which cannot represent the realistic nonlinear heating (positive-only heating) effect, thus the wave selection is obtained for both circulation and precipitation.

4. Summary and discussion

This work extends the MJO skeleton model of MS09 and LW12 into an air–sea coupled conceptual model, which demonstrates that the air–sea interaction under mean westerly winds induces coupled instability and selects the eastward planetary-scale propagation as the most favored mode. Besides the air–sea coupling, the frictional boundary layer moisture convergence also presents an instability source for the planetary-scale eastward propagation in the skeleton model (LW12). Although some works reported that the air–sea coupling may not be a key for the poor MJO simulation in models (Hendon 2000; Newman et al. 2009), our results show the positive role of the air–sea interaction in sustaining the MJO and present a mechanism for explaining why the MJO has been observed to have eastward propagation on preferred planetary scales. Meanwhile, the mean westerly winds are the necessary condition for the air–sea coupling to provide an instability source for the eastward modes.

Without a planetary boundary layer, the air–sea interaction processes, through changing shortwave radiation, evaporation, and ocean entrainment, destabilize all wavelengths in the model, including the smallest wavelength and both eastward and westward modes. The Rossby waves are almost independent of wavenumber (Fig. 1). The presence of a frictional boundary layer will remedy these deficiencies (LW12). Compared to the pure air–sea interaction (Fig. 1), the inclusion of a frictional boundary layer gives more realistic solutions (Fig. 7). The frictional boundary layer moisture convergence selects long eastward modes, which have the strongest growth rate, and damps long westward modes. Compared to long eastward modes, the instability of the smallest wavelengths is very weak, which shows that the long eastward mode is the preferred mode, which is relevant to understanding the development and maintenance of the MJO against dissipation.

This frictional air–sea coupled skeleton model presents a simple linear tool to study the MJO, and the mean states in the atmosphere (Wang and Xie 1997) can also be implemented into this model. Here, we focus on the role of air–sea interaction in the MJO, and thus the role of wind–evaporation feedback in the atmosphere is not

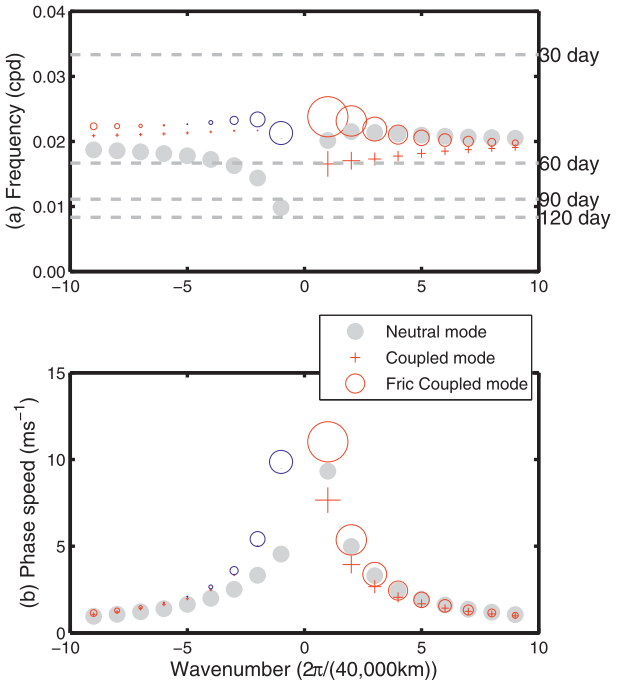

FIG. 7. Growth rate and phase speed for air–sea coupled skeleton mode in the presence of the boundary layer friction. As in Fig. 1, but crosses denote solutions with the frictional boundary layer included. The maximum and minimum growth rates are 0.12 and $-0.06\,\text{day}^{-1}$, respectively. Negative growth rates are denoted by blue circles. The frictional boundary layer damps the long westward mode while preferring the long eastward mode.

included. Different from the original linear wind-induced surface heat exchange (Emanuel, 1987, Neelin et al. 1987), where mean easterly drives eastward propagation, the strong asymmetric westerly anomalies of the MJO can also enhance the MJO under the mean westerly winds (Maloney et al. 2010). This latter mechanism included in this air–sea coupled model may leads to more realistic MJO simulation.

Acknowledgments. This study has been supported by Climate Dynamics Program of the National Science Foundation under Award AGS-1005599, the NOAA/MAPP project Award NA10OAR4310247, and APEC climate center. Additional support was provided by the Japan Agency for Marine-Earth Science and Technology (JAMSTEC) through their sponsorship of research activities at the International Pacific Research Center.

REFERENCES

Davey, M. K., and A. E. Gill, 1987: Experiments on tropical circulation with a simple moist model. *Quart. J. Roy. Meteor. Soc.,* **113,** 1237–1269.

Emanuel, K. A., 1987: An air–sea interaction model of intraseasonal oscillations in the tropics. *J. Atmos. Sci.,* **44,** 2324–2340.

Flatau, M., P. J. Flatau, P. Phoebus, and P. P. Niiler, 1997: The feedback between equatorial convection and local radiative and evaporative processes: The implications for intraseasonal oscillations. *J. Atmos. Sci.,* **54,** 2373–2386.

Hendon, H. H., 2000: Impact of air–sea coupling on the Madden–Julian oscillation in a general circulation model. *J. Atmos. Sci.,* **57,** 3939–3952.

——, and M. L. Salby, 1994: The life cycle of the Madden–Julian oscillation. *J. Atmos. Sci.,* **51,** 2225–2237.

——, and J. Glick, 1997: Intraseasonal air–sea interaction in the tropical Indian and Pacific oceans. *J. Climate,* **10,** 647–661.

Hirst, A. C., 1986: Unstable and damped equatorial modes in simple coupled ocean–atmosphere models. *J. Atmos. Sci.,* **43,** 606–630.

Houze, R. A., Jr., S. S. Chen, D. E. Kingsmill, Y. Serra, and S. E. Yuter, 2000: Convection over the Pacific warm pool in relation to the atmospheric Kelvin–Rossby wave. *J. Atmos. Sci.,* **57,** 3058–3089.

Inness, P. M., J. M. Slingo, E. Guilyardi, and J. Cole, 2003: Simulation of the Madden–Julian oscillation in a coupled general circulation model. Part II: The role of the basic state. *J. Climate,* **16,** 365–382.

Jones, C., D. E. Waliser, and C. Gautier, 1998: The influence of the Madden–Julian oscillation on ocean surface heat fluxes and sea surface temperature. *J. Climate,* **11,** 1057–1072.

Kawamura, R., 1988: Intraseasonal variability of sea surface temperature over the tropical western Pacific. *J. Meteor. Soc. Japan,* **66,** 1007–1012.

Khouider, B., and A. J. Majda, 2006: A simple multicloud parameterization for convectively coupled tropical waves. Part I: Linear analysis. *J. Atmos. Sci.,* **63,** 1308–1323.

——, and ——, 2008: Equatorial convectively coupled waves in a simple multicloud model. *J. Atmos. Sci.,* **65,** 3376–3397.

Kikuchi, K., and B. Wang, 2010: Spatiotemporal wavelet transform and the multiscale behavior of the Madden–Julian oscillation. *J. Climate,* **23,** 3814–3834.

Kiladis, G. N., K. H. Straub, and P. T. Haertel, 2005: Zonal and vertical structure of the Madden–Julian oscillation. *J. Atmos. Sci.,* **62,** 2790–2809.

Knutson, T. R., and K. M. Weickmann, 1987: 30-60-day atmospheric oscillation: Composite life cycles of convection and circulation anomalies. *Mon. Wea. Rev.,* **115,** 1407–1436.

Krishnamurti, T. N., D. K. Oosterhof, and A. V. Mehta, 1988: Air–sea interaction on the time scale of 30 to 50 days. *J. Atmos. Sci.,* **45,** 1304–1322.

Lau, K. M., and C. H. Sui, 1997: Mechanisms of short-term sea surface temperature regulation: Observations during TOGA COARE. *J. Climate,* **10,** 465–472.

Lindzen, R. S., and S. Nigam, 1987: On the role of the sea surface temperature gradients in forcing low-level winds and convergence in the Tropics. *J. Atmos. Sci.,* **44,** 2440–2458.

Liu, F., and B. Wang, 2012a: A frictional skeleton model for the Madden–Julian oscillation. *J. Atmos. Sci.,* **69,** 2749–2758.

——, and ——, 2012b: A model for the interaction between 2-day waves and moist Kelvin waves. *J. Atmos. Sci.,* **69,** 611–625.

——, and ——, 2012c: Impacts of upscale heat and momentum transfer by moist Kelvin waves on the Madden–Julian oscillation: A theoretical model study. *Climate Dyn.,* **40,** 213–224, doi:10.1007/s00382-011-1281-0.

——, and ——, 2012d: A conceptual model for self-sustained active-break Indian summer monsoon. *Geophys. Res. Lett.,* **39,** L20814, doi:10.1029/2012GL053663.

Madden, R. A., and P. Julian, 1971: Detection of a 40–50-day oscillation in the zonal wind in the tropical Pacific. *J. Atmos. Sci.,* **28,** 702–708.

Majda, A. J., and S. N. Stechmann, 2009: The skeleton of tropical intraseasonal oscillations. *Proc. Natl. Acad. Sci. USA,* **106,** 8417–8422.

——, and ——, 2011: Nonlinear dynamics and regional variations in the MJO skeleton. *J. Atmos. Sci.,* **68,** 3053–3071.

Maloney, E. D., and D. L. Hartmann, 1998: Frictional moisture convergence in a composite life cycle of the Madden–Julian oscillation. *J. Climate,* **11,** 2387–2403.

——, A. H. Sobel, and W. M. Hannah, 2010: Intraseasonal variability in an aquaplanet general circulation model. *J. Adv. Model. Earth Syst.,* **2,** 1–24.

Moncrieff, M. W., 2004: Analytic representation of the large-scale organization of tropical convection. *J. Atmos. Sci.,* **61,** 1521–1538.

Nakazawa, T., 1988: Tropical super clusters within intraseasonal variations over the western Pacific. *J. Meteor. Soc. Japan,* **66,** 823–836.

Neelin, J. D., 1989: On the interpretation of the Gill model. *J. Atmos. Sci.,* **46,** 2466–2468.

——, I. M. Held, and K. H. Cook, 1987: Evaporation–wind feedback and low-frequency variability in the tropical atmosphere. *J. Atmos. Sci.,* **44,** 2341–2348.

Newman, M., P. D. Sardeshmukh, and C. Penland, 2009: How important is air–sea coupling in ENSO and MJO evolution? *J. Climate,* **22,** 2958–2977.

Philander, S. G. H., T. Yamagata, and R. C. Pacanowski, 1984: Unstable air–sea interactions in the tropics. *J. Atmos. Sci.,* **41,** 604–613.

Roundy, P. E., and W. Frank, 2004: A climatology of waves in the equatorial region. *J. Atmos. Sci.,* **61,** 2105–2132.

Rui, H., and B. Wang, 1990: Development characteristics and dynamic structure of tropical intraseasonal convection anomalies. *J. Atmos. Sci.,* **47,** 357–379.

Salby, M. L., and H. H. Hendon, 1994: Intraseasonal behavior of clouds, temperature, and motion in the tropics. *J. Atmos. Sci.,* **51,** 2207–2224.

Slingo, A., P. Inness, R. Neale, S. Woolnough, and G.-Y. Yang, 2003: Scale interaction on diurnal to seasonal timescales and their relevance to model systematic errors. *Ann. Geophys.,* **46,** 139–155.

Waliser, D. E., K. M. Lau, and J. H. Kim, 1999: The influence of coupled sea surface temperatures on the Madden–Julian oscillation: A model perturbation experiment. *J. Atmos. Sci.,* **56,** 333–358.

Wang, B., and H. Rui, 1990a: Synoptic climatology of transient tropical intraseasonal convection anomalies. *Meteor. Atmos. Phys.,* **44,** 43–61.

——, and ——, 1990b: Dynamics of the coupled moist Kelvin–Rossby wave on an equatorial beta-plane. *J. Atmos. Sci.,* **47,** 397–413.

——, and T. Li, 1993: A simple tropical atmosphere model of relevance to short-term climate variation. *J. Atmos. Sci.,* **50,** 260–284.

——, and ——, 1994: Convective interaction with boundary-layer dynamics in the development of a tropical intraseasonal system. *J. Atmos. Sci.,* **51,** 1386–1400.

——, and X. Xie, 1997: A model for the boreal summer intraseasonal oscillation. *J. Atmos. Sci.,* **54,** 72–86.

——, and ——, 1998: Coupled modes of the warm pool climate system. Part I: The role of air–sea interaction in maintaining Madden–Julian oscillation. *J. Climate,* **11,** 2116–2135.

——, T. Li, and P. Chang, 1995: An intermediate model of the tropical Pacific Ocean. *J. Phys. Oceanogr.,* **25,** 1599–1616.

——, P. J. Webster, and H. Teng, 2005: Antecedents and self-induction of the active-break south Asian monsoon unraveled by satellites. *Geophys. Res. Lett.,* **32,** L04704, doi:10.1029/2004GL020996.

Wheeler, M., and G. N. Kiladis, 1999: Convectively coupled equatorial waves: Analysis of clouds and temperature in the wavenumber-frequency domain. *J. Atmos. Sci.,* **56,** 374–399.

Zebiak, S. E., 1986: Atmospheric convergence feedback in a simple model for El Niño. *Mon. Wea. Rev.,* **114,** 1263–1271.

Zhang, C., 1996: Atmospheric intraseasonal variability at the surface in the western Pacific Ocean. *J. Atmos. Sci.,* **53,** 739–785.

——, 2005: Madden–Julian oscillation. *Rev. Geophys.,* **42,** G2003, doi:10.1029/2004RG000158.

——, and M. Dong, 2004: Seasonality of the Madden–Julian oscillation. *J. Climate,* **17,** 3169–3180.

Zhou, L., R. B. Neale, M. Jochum, and R. Murtugudde, 2012: Improved Madden–Julian oscillations with improved physics: The impact of modified convection parameterizations. *J. Climate,* **25,** 1116–1136.